

See discussions, stats, and author profiles for this publication at: <https://www.researchgate.net/publication/366529940>

# Experimental Assessment of Variation in Open Area Ratio on Thermohydraulic Performance of Parallel Flow Solar Air Heater List of Symbols

Article in ARABIAN JOURNAL FOR SCIENCE AND ENGINEERING · December 2022

DOI: 10.1007/s13369-022-07525-7

CITATIONS

11

READS

41

6 authors, including:



**Varun Pratap Singh**

University of Petroleum & Energy Studies

45 PUBLICATIONS 246 CITATIONS

[SEE PROFILE](#)



**Siddharth Jain**

College of Engineering Roorkee

78 PUBLICATIONS 3,345 CITATIONS

[SEE PROFILE](#)



**Gaurav Dwivedi**

Maulana Azad National Institute of Technology, Bhopal

155 PUBLICATIONS 3,313 CITATIONS

[SEE PROFILE](#)



**Tabish Alam**

Central Building Research Institute

73 PUBLICATIONS 1,212 CITATIONS

[SEE PROFILE](#)

Some of the authors of this publication are also working on these related projects:



Advanced Numerical Simulations in Mechanical Engineering [View project](#)



Advances in Sustainable Machining and Manufacturing Processes [View project](#)



# Experimental Assessment of Variation in Open Area Ratio on Thermohydraulic Performance of Parallel Flow Solar Air Heater

Varun Pratap Singh<sup>1</sup> · Siddharth Jain<sup>1</sup> · Ashish Karn<sup>1</sup> · Gaurav Dwivedi<sup>2</sup> · Tabish Alam<sup>3</sup> · Ashwani Kumar<sup>4</sup>

Received: 24 July 2022 / Accepted: 27 November 2022  
© King Fahd University of Petroleum & Minerals 2022

## Abstract

This experimental study explains the phenomena of secondary flow development due to change in rib perforation and the effect on improvement in THPP values due to variation in  $\beta$  and  $W/w$  values of a perforated multi-V rib roughness applied in double-pass parallel flow solar air heater (DPPFSAH). The fixed parameters are  $e/D = 0.043$ ,  $p/e = 10$ ,  $\alpha = 60^\circ$  and  $W/H = 12$ , and the range of variable parameters includes  $\beta = 0.0-0.31$ ,  $W/w = 2-10$  and  $Re = 2000-18,000$ . The optimum values of  $Nu/Nu_s$ ,  $f/f_s$ , THPP and TEIF are observed as 9.66, 12.31, 3.96 and 1.33, respectively, at  $\beta = 0.27$  and  $W/w = 6$ . The maximum improvement in THPP values was 3.96 times and 1.90 times in DPPFSAH with perforation and continuous rib with a smooth plate, respectively. Double-pass SAH outperforms the single-pass SAH. Correlations for  $Nu$  and  $f$  are also developed for DPPFSAH with  $\pm 14\%$  and  $\pm 7\%$  accuracy.

**Keywords** Solar energy · Solar air heater · Double pass · Perforated rib · Multi-V rib

## List of Symbols

$A$	Area ( $m^2$ )
$D$	Diameter (m)
$e$	Rib height (m)
$H$	Duct height (m)
$h$	Convective coefficient of heat transfer ( $W/m^2K$ )

$I$	Average insolation ( $W/m^2$ )
$L$	Duct length (m)
$\dot{m}$	Mass flow rate (kg/s)
$P$	Pressure (Pa)
$T$	Temperature (K)
$w$	Rib width (m)
$W$	Duct width (m)

✉ Varun Pratap Singh  
ray\_varun@yahoo.com

Siddharth Jain  
arthjain2001@gmail.com

Ashish Karn  
akarn@ddn.upes.ac.in

Gaurav Dwivedi  
gdiitr2005@gmail.com

Tabish Alam  
tabish.iitr@gmail.com

Ashwani Kumar  
drashwanikumardte@gmail.com

- <sup>1</sup> Department of Mechanical Engineering, SoE, UPES, Dehradun, India
- <sup>2</sup> Energy Centre, MANIT, Bhopal 462 003, India
- <sup>3</sup> Building Energy Efficiency Division, CSIR-CBRI, Roorkee 247667, India
- <sup>4</sup> Technical Education Department Uttar Pradesh, Kanpur, India

## Subscripts

$d$	Duct/channel, diameter
$m$	Mean
$s$	Smooth
$h$	Hydraulic
$th$	Thermal

## Dimensionless parameters

$D_o/D_p$	Orifice diameter ratio
$e/D_h$	Relative roughness height
$f/f_s$	Friction factor ratio
$Nu/Nu_s$	Nusselt number ratio
$W/H$	Duct aspect ratio
$W/w$	Relative roughness width



Re Reynolds number

## Greek symbols

$\Delta$	Drop, gradient
$\eta$	Efficiency
$\beta$	Open area ratio, duct slop
$\mu$	Dynamic viscosity (Pa·s)
$\theta$	Manometer slop
$\alpha$	Attack angle (°)
THPP	Thermohydraulic performance parameter
DPPF	Double-pass parallel flow
SAH	Solar air heater

## Abbreviations

THPP	Thermohydraulic performance parameter
DPPF	Double-pass parallel flow
SAH	Solar air heater

## 1 Introduction

Solar air heat technology may be used in several applications to minimize the carbon footprint of traditional heating systems, including fossil fuels, and offer a more sustainable way to generate thermal energy. A traditional solar air heater (SAH) typically having a flat wooden duct with a base plate having synthetic roughness, a transparent glazing and insulating material on the base and side-wise. SAH applications are usually limited to low-temperature gradient uses such as water heating, room heating, crop drying, agricultural season extensions, preheating, process heating, commercial ventilation makeup air, air conditioning and space heating and cooling [1, 2]. SAH's usage in low-temperature gradient applications can be ascribed to the reduced heat transfer between air and the roughened absorber plate, which is caused by the reduced convection heat transfer coefficient. Several studies have focused on different strategies to enhance the convection coefficient by employing a variety of design options with different roughness geometry and to analyse the SAH thermohydraulic performance parameter (THPP) [3].

The basic methods used by researchers to increase the single-pass SAH (SPSAH) performance were variations in geometry parameters, operation parameters and the addition of the number of passes of fluid flow [4, 5]. Since the application of double-pass SAH (DPSAH) increases the collector surface area, it offers considerable gains in heat transfer [6].

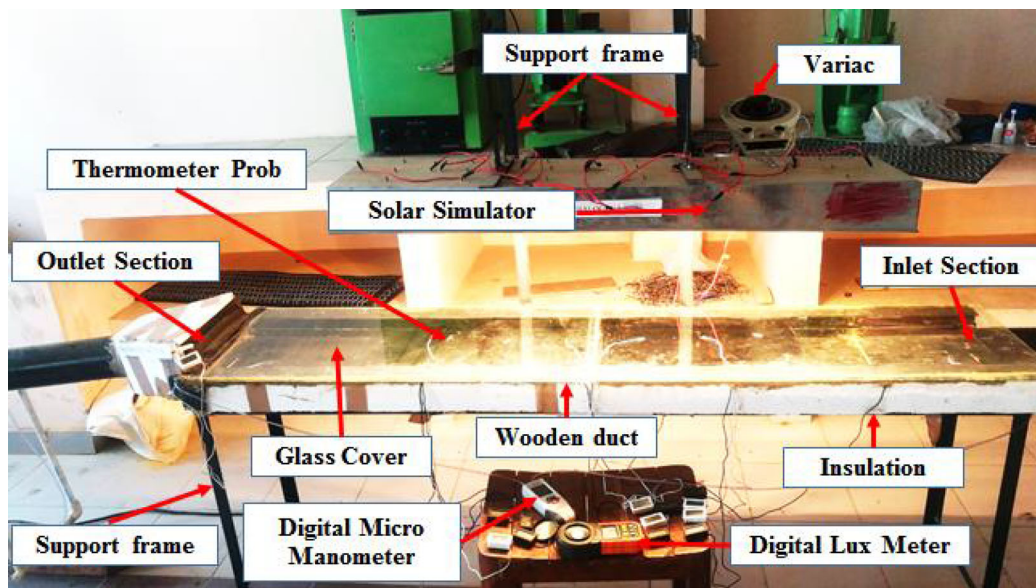
Double-pass SAH with cross-flow [7, 8], recycling [9] and parallel flow [10] are different DPSAH arrangements that were used as the primary factors that affected the performance [11–13].

Besides these reports, several researchers have focused specifically on the effect of ribs and baffles on the heat transfer enhancement over a smooth SAH. As per the literature, the most influencing parameters in rib roughness include relative roughness height ( $e/D_h$ ), relative roughness pitch ( $p/e$ ), angle of attack ( $\alpha$ ), aspect ratio ( $W/H$ ), collector slope ( $\beta$ ) and rib geometry [13–19]. For multiple V-shaped ribs, Arya et al. [20–22], Tabish et al. [23, 24] Ravi and Saini [25, 26], Singh and Kaur [27] and Kumar et al. [17, 28] have determined the optimum configuration variable combinations for multi-V rib configuration. When compared to SPSAH, Ravi and Saini [26] found that the DPSAH improved the Nusselt number ratio ( $Nu/Nu_s$ ) by 3.4 times and the friction factor ratio ( $f/f_s$ ) by 2.5 times. Thakur and Thakur [29] observed a 2.3–4.1 times improvement in  $Nu$  value by applying W-shaped ribs with staggering as compared to a smooth SAH. Singh et al. [30, 31] analysed the effect of perforation with continuous rib in multi-V geometry in SPSAH and DPPF-SAHA and observed significant improvement because of the application of perforations. Singh et al. [32, 33] investigated the effect of variation in  $\beta$  and  $W/w$  for a distinct set of perforated multi-V ribs and found that the effectiveness of SPSAH improved significantly.

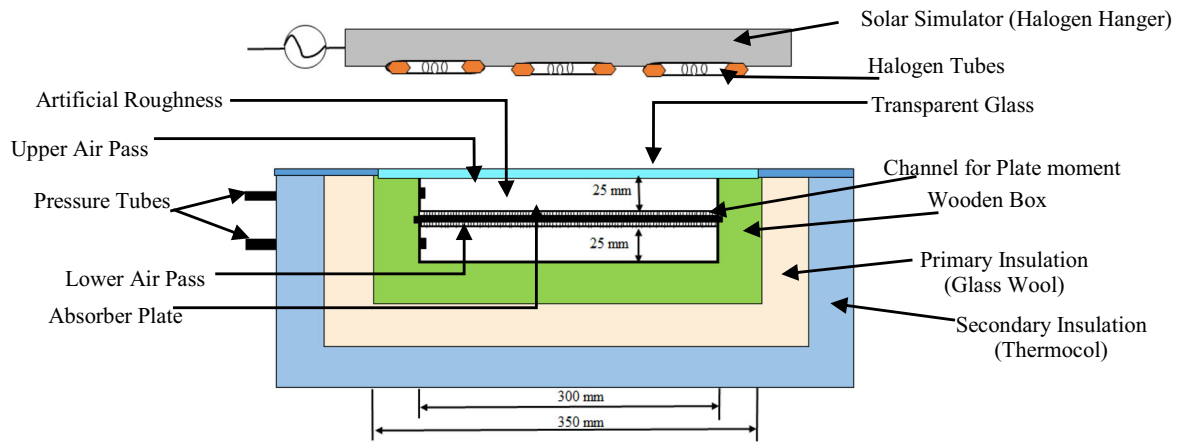
A review by Hernández and Quinonez [34] reveals that the application of DPPFSAH reduces drag forces to a minimal level, which handles high pumping power while having optimum thermal effectiveness. The rapid air flow rate of the supplementary streams via holes creates more turbulence during detachment and reattachment, which enhances the THP of SAH [35]. Because of the high airflow rate via secondary passages, DPPFSAH's perforated multi-V ribbed rough surfaces can play an essential role in improving  $Nu$  and reducing  $f$  values. The aim of the current study is to analyse the effects of variation in  $\beta$  and  $W/w$  values on THP for DPPFSAH and compare it with the SPSAH studied by Singh et al. [32] and other researchers. The current research thus seeks to explore the effect of perforations in ribs on the performance of DPPSAH.

## 2 Set-up Configuration and Roughness Parameter Details

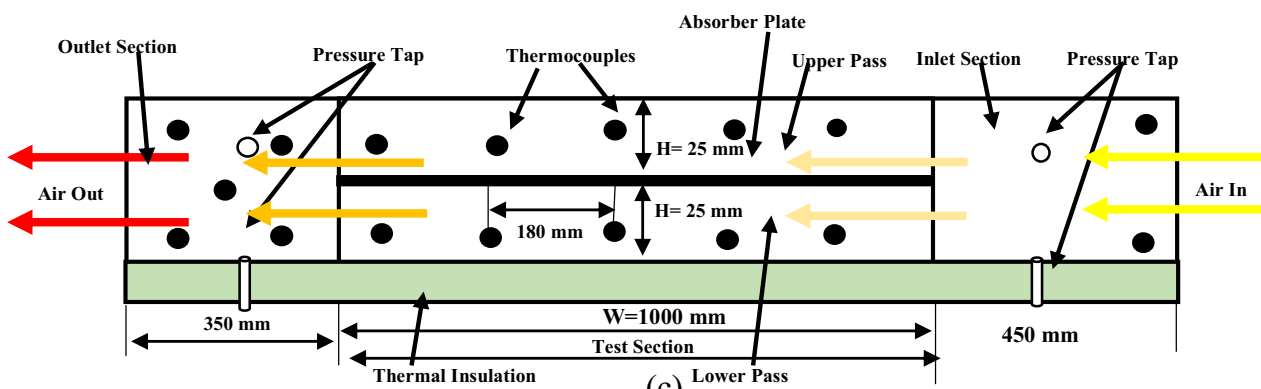
A DPPFSAH set-up (Fig. 1a–c) is fabricated as per the ASHRAE standard (ASHRAE 93-77, 1977). The detailed description of set-up, fixed and variable parameters is mentioned in detail in earlier research work [31] and mentioned in Table 1.



(a)



(b)



(c)

Fig. 1 a Experimental set-up, b cross-sectional view and c thermocouple and pressure tap placement in DPPFSAH [31]

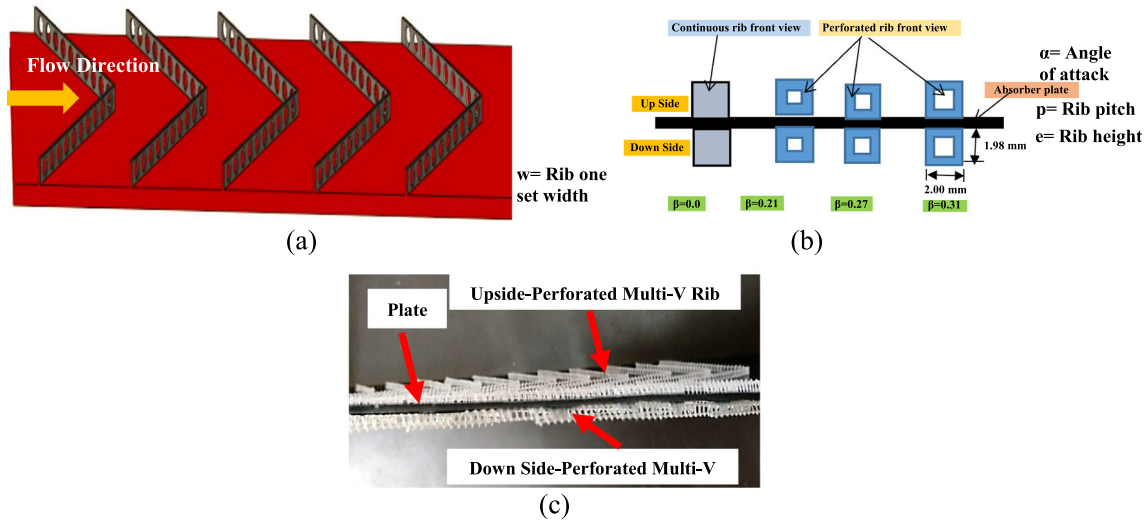


**Fig. 2** a Parameter denotation on multi-V perforated plate, b front view of ribs with variation in  $\beta$ , c perforated V-shaped roughness rib arrangements on both sides of the base plate

**Table 1** Parameters being used in the study are listed below

Parameter notation with unit	Value
$W$ (m)	0.3
$H$ (m)	0.025
$W/H$	12
$D_o/D_p$	0.55
$D_h$ (m)	0.04615
$e$ (m)	0.002
$e/D$	0.043
$p/e$	10
$\alpha$ ( $^\circ$ )	60
$W/w$	2: 2:10
$\beta$	0.0, 0.21, 0.27, 0.31
Re	2000:2000:18,000
$I$ ( $W/m^2$ )	800
Rib type	Multi-V ribs
Rib material	GI wire (continuous rib), PVC (perforated rib)

Figure 2a–c gives a visual representation of perforated multi-V rib roughness geometry taken up in this study.

### 3 Data Handling

Although the detailed description of the governing equations and data handling is discussed in the preceding work by the authors [31], the same equations are mentioned here in brief, for the improved readability of the current paper. The THP values were calculated by averaging the data values. The

average temperature of base plate  $T_{pmean}$  can be calculated as [36]:

$$T_{pmean} = \frac{1}{18} \left( \sum_{i=1}^{18} T_i \right) \quad (1)$$

The average air temperature  $T_{amean}$  can be found as:

$$T_{amean} = \frac{T_{in} + T_{out}}{2} \quad (2)$$

where  $T_{in} = \frac{T_{in1} + T_{in2}}{2}$  and

$$T_{out} = \frac{T_{out1} + T_{out2} + T_{out3} + T_{out4} + T_{out5}}{5} \quad (3)$$

Air mass flow rate is measured by:

$$\dot{m} = c_d A_o \sqrt{\frac{2\rho(\Delta P_o)}{1 - (D_o/D_p)^4}} \quad (4)$$

where

$$\Delta P_o = \rho_m g \Delta h_o \sin \theta \quad (5)$$

The velocity of air is considered as:

$$V = m/\rho WH \quad (6)$$

Channel hydraulic diameter ( $D_h$ ) can be found as:

$$D_h = 4WH/2(W + H) \quad (7)$$

Test section friction factor ( $f$ ) can be calculated as:

$$f = 2(\Delta p)_d D_h / 4\rho L v^2 \tag{8}$$

The heat transfer coefficient ( $h$ ) is defined as:

$$h = Q_u / A_p (T_{pm} - T_{fm}) \tag{9}$$

The useful heat gain ( $Q_u$ ) is measured as:

$$Q_u = \dot{m} c_p (T_{out} - T_{in}) \tag{10}$$

By Eqs. (7) and (9), the Nusselt number is [37]:

$$Nu = h D_h / K \tag{11}$$

The Reynolds number ( $Re$ ) is measured as:

$$Re = V D_h / \nu \tag{12}$$

Finally, the DPPFSAH thermal efficiency ( $\eta_{thermal}$ ) was obtained as:

$$\eta_{thermal} = \dot{m} C_p \Delta T / I A_p \tag{13}$$

### 4 Validation of Experimental Set-ups and Analysis of Uncertainties

An experimental set-up of DPPFSAH having a smooth plate with  $Re$  in the range of 2000–18,000 was tested for the validation study. The measured values of  $Nu_s$  and  $f_s$  are put in comparison with the revised Dittus–Boelter and revised Blasius equations, respectively [38].

By modified Dittus–Boelter equation:

$$Nu_s = 0.024 Re^{0.8} Pr^{0.4} \tag{14}$$

Modified Blasius equation:

$$f_s = 0.085 Re^{-0.025} \tag{15}$$

An illustrative connection between empirical and theoretical  $Nu_s$  and  $f_s$  results for  $Re$  is shown in Fig. 3.

The  $Nu_s$ ,  $f_s$  and  $Re$  were calculated using empirically collected data, including airflow, intake and exit average temperature, solar irradiation and pressure losses. For error analysis, this study uses the Kline and McClintock [39] method. The author provides a detail of uncertainty calculation in the earlier published work [32]. The mean error percentages of  $Nu$ ,  $Re$  and  $f$  are observed as  $\pm 1.83\%$ ,  $\pm 1.65\%$  and  $\pm 3.28\%$ , respectively.

## 5 Results and Discussions

The assessment of design and performance variables on the THPP of DPPFSAH that has been artificially roughened using perforated multi-V ribs was investigated and analysed.

### 5.1 Near-wall flow development

Figure 4A, b shows how perforation in a multi-V rib causes complicated fluid flow patterns at the wall surfaces when compared to an unbroken rib. The fluid flow area and stream reattachment interval beneath the ribs limit the quantity of transferred energy from the base plate [40]. Geometry parameters drive the THP enhancements, which may be addressed through Reynolds number ( $Re$ ), rib roughness and duct characteristics. In perforated ribs, the zone of reattachment shrinks, and the growth of upstream and downstream vertices reduces, leading to even more close connections for fresh fluid flow with the heated surface and improved thermal interaction inside the reattachment zone [41].

The stream’s mixing between the two neighbouring perforated ribs and front vortices is also improved by perforation in the ribs, allowing it to flow alongside it. Tariq et al. [42] suggest that this improves flow capacity and lowers pressure drop, leading to less pumping power required to sustain fluid flow. Furthermore, the perforation allows cooler secondary air to easily replace trapped air in the vortex that combines it with the main flow, enhancing heat transfer beyond the ribs. Perforation promotes mixing throughout the rib and plate contact area and lowers vortices for smaller Reynolds numbers. It can accelerate the levels of turbulent mixing in the stream. Figure 5a, b shows this phenomenon of producing turbulence between the two consecutive ribs. As a result of the increased turbulence, rib perforation rises THP.

### 5.2 Effect of Operating Variables

In this section, the influence of different variables is studied by maintaining the other parameters’ values unchanged. The changes in varying parameters have been mapped with  $Re$ ,  $W/w$  and  $\beta$ , and their effects are described and analysed in detail.

#### 5.2.1 Effect of Reynolds Number ( $Re$ )

Because of a substantial improvement in mixing and turbulence in the secondary stream attributed to the perforations, Fig. 6a–d demonstrates a substantial enhancement in  $Nu$  values for higher values of  $Re$ , resulting in a larger  $Nu$  and enhanced thermal outcomes of DPPFSAH. In DPPFSAH, at  $\beta = 0.27$ , the optimal value of  $Nu$  is 556.19 for  $W/w = 6$  at  $Re = 18,000$ , respectively. Figure 8a indicates the comparison between  $Nu$  for different  $\beta$  values at  $W/w = 6$  for perforated

**Fig. 3**  $Nu_s$  and  $f_s$  measured and theoretical results for a smooth DPPFSAH

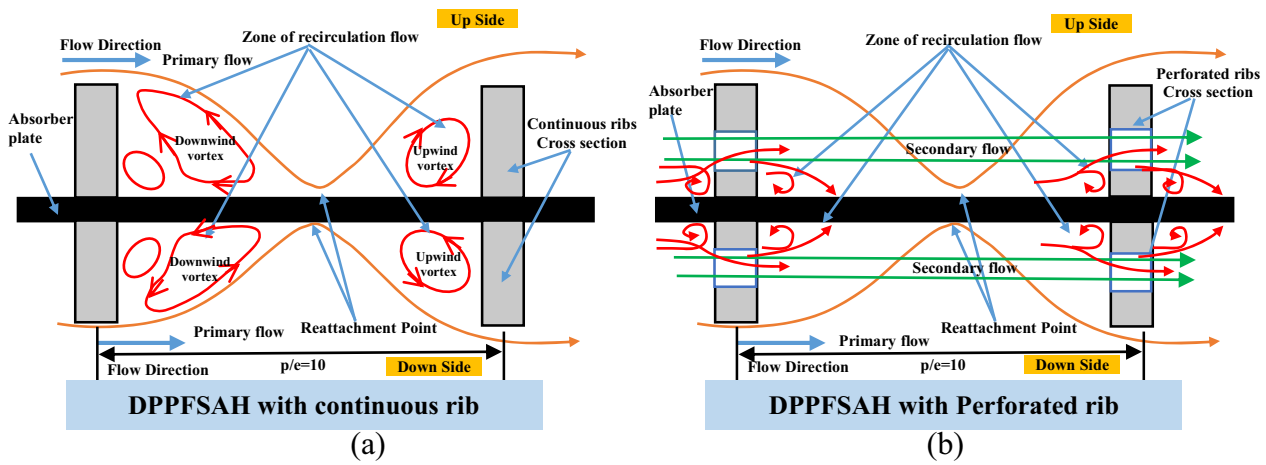
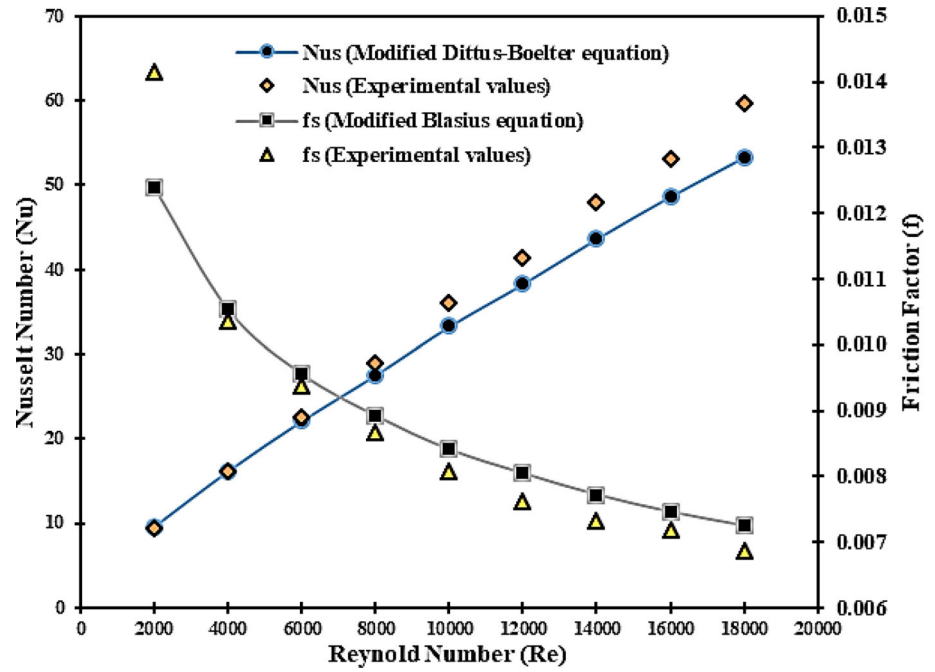


**Fig. 4** Near-wall flow development of **a** continuous rib ( $\beta = 0.0$ ) [41], **b** perforated rib [42]

multi-V rib and the flat duct in SPSAH and DPPFSAH, and it is clearly evident that the roughened DPPFSAH outperforms the roughened SPSAH in all cases. Figure 7a–d explains the change in  $f$  value with different  $\beta$  values for a range of  $Re$  in the DPPFSAH and shows a considerable reduction because of additional flow developed due to perforated ribs, which decreases the flow barrier and decreases energy requirement. The minimal value of  $f = 0.04476$  is shown in DPPFSAH with  $\beta = 0.31$  at  $W/w = 2$  and  $Re = 18,000$ . Figure 8b shows the comparison between different  $f$  values for different  $\beta$  values at  $W/w = 6$  in SPSAH and DPPFSAH. SPSAH with roughness shows minimum values for friction factor as compared to DPPFSAH in all cases. Under the same operating circumstances, perforation in multi-V ribs reduces energy consumption significantly.

**5.2.2 Effect of Relative Roughness Width ( $W/w$ )**

Figure 9a–d illustrates the influence of  $W/w$  on  $Nu$  for different  $\beta$  values, and the figure indicates that increasing  $W/w$  initially improves  $Nu$  in all four conditions, attaining a maximum value at  $W/w = 6$ , and any additional rise in the  $W/w$  decreases the  $Nu$  value. It is expected that, at  $W/w = 6$ , flow mixing induced due to the proposed geometry has attained its maximum value and any further rise in  $W/w$  could disrupt the improvement in secondary flow due to flatness growth in roughness geometry and reduce rib effectiveness, which reduces thermal effectiveness. While Fig. 10a–d illustrates the influence of  $W/w$  on  $f$ , the  $f$  value regularly increases with an augmentation in  $W/w$  value due to the turbulence formed in the flow.

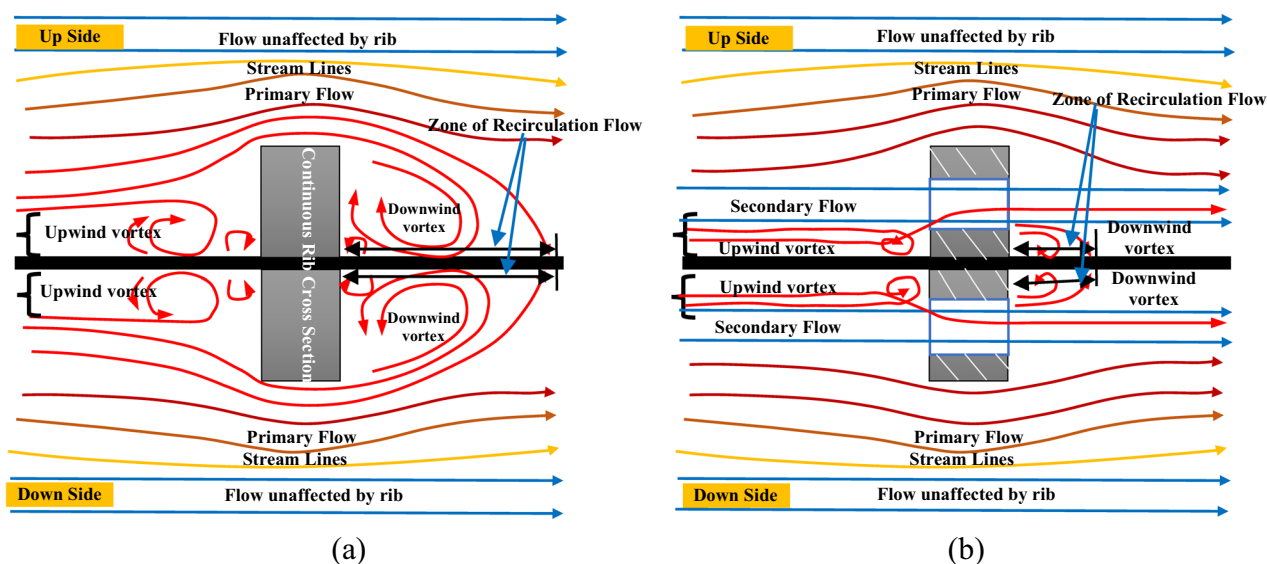


Fig. 5 Flow movement and development of vortices a continuous rib, b perforated rib in the DPPPSAH duct [42]

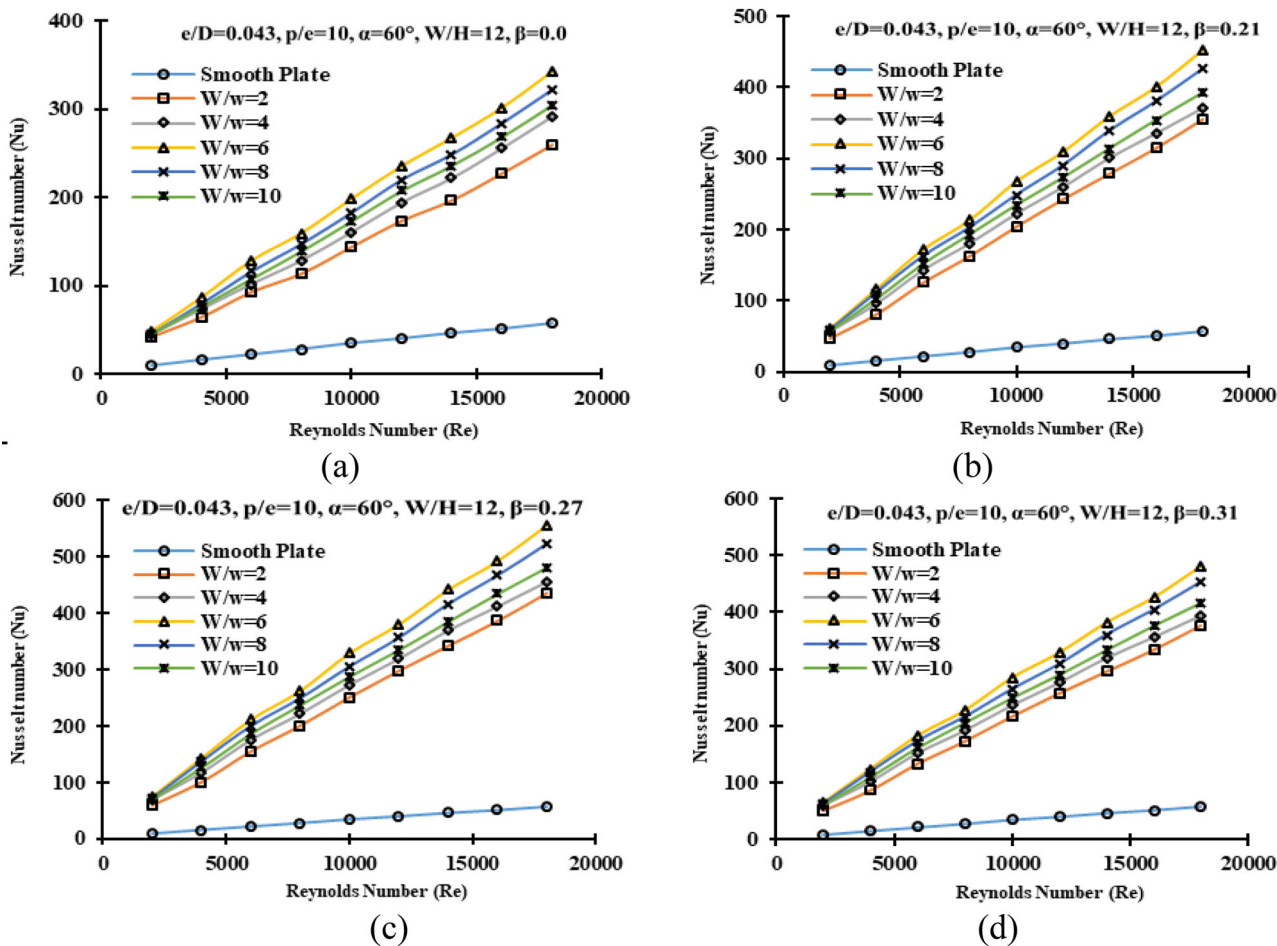
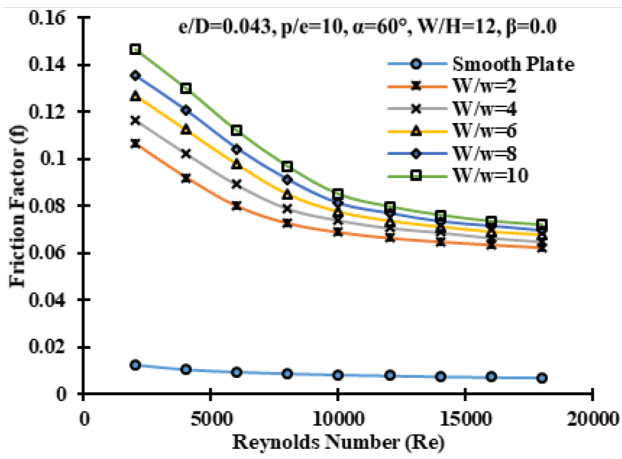
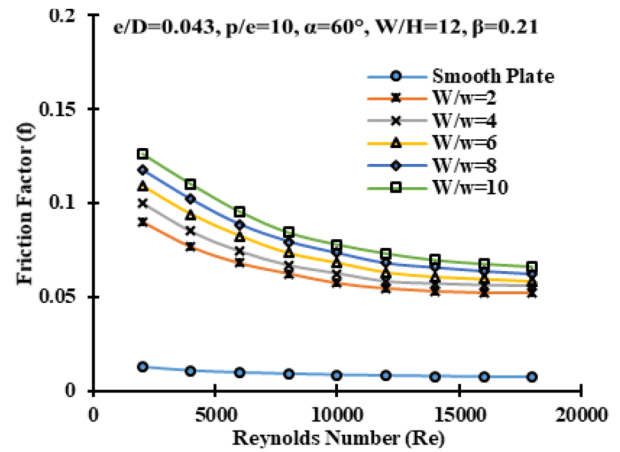


Fig. 6 Influence of Re on Nu for different  $\beta$  value a 0.0, b 0.21, c 0.27 and d 0.31 at different  $W/w$  values in DPPPSAH

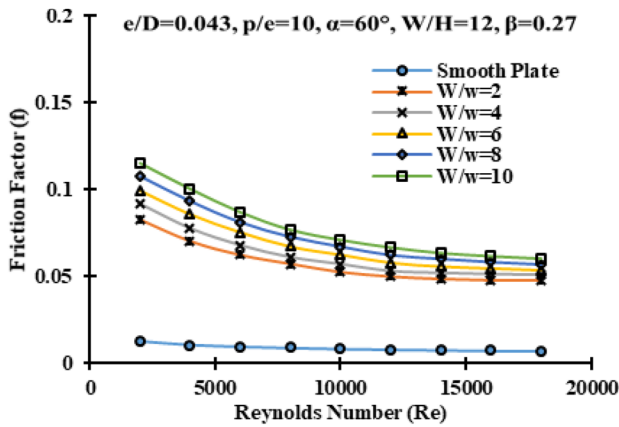




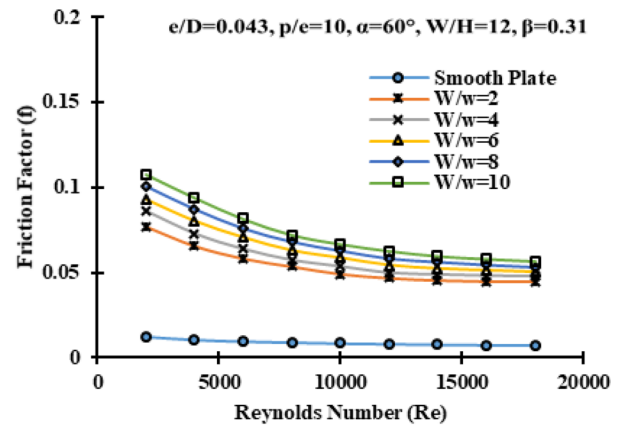
(a)



(b)

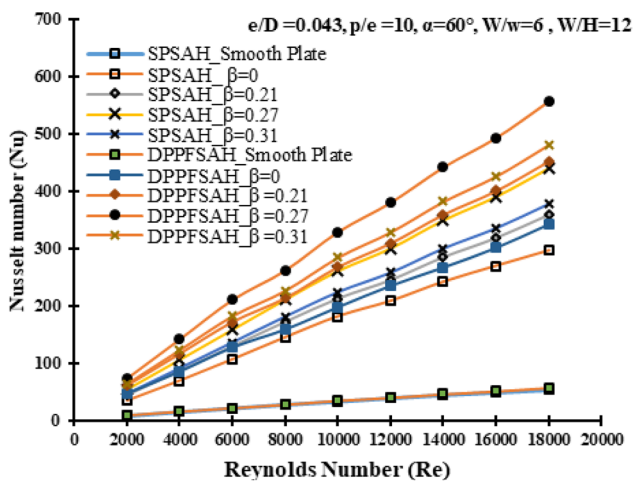


(c)

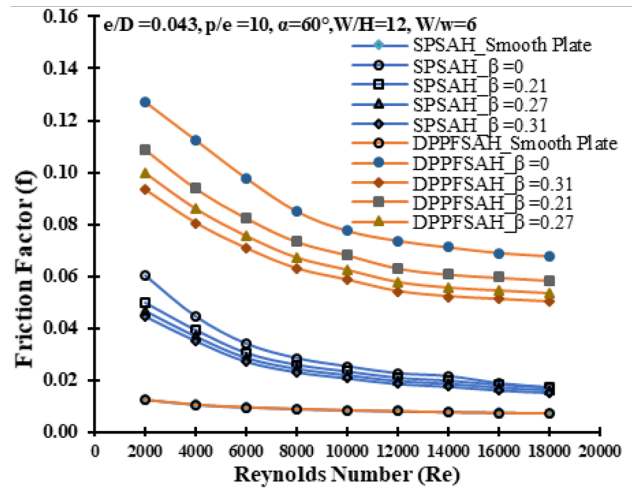


(d)

Fig. 7 Influence of Re on  $f$  for different  $\beta$  value a 0.0, b 0.21, c 0.27 and d 0.31 for different  $W/w$  values in DPPFSAH



(a)



(b)

Fig. 8 Comparison between a Nu and Re and b  $f$  and Re of SPSAH and DPPFSAH for different  $\beta$  values

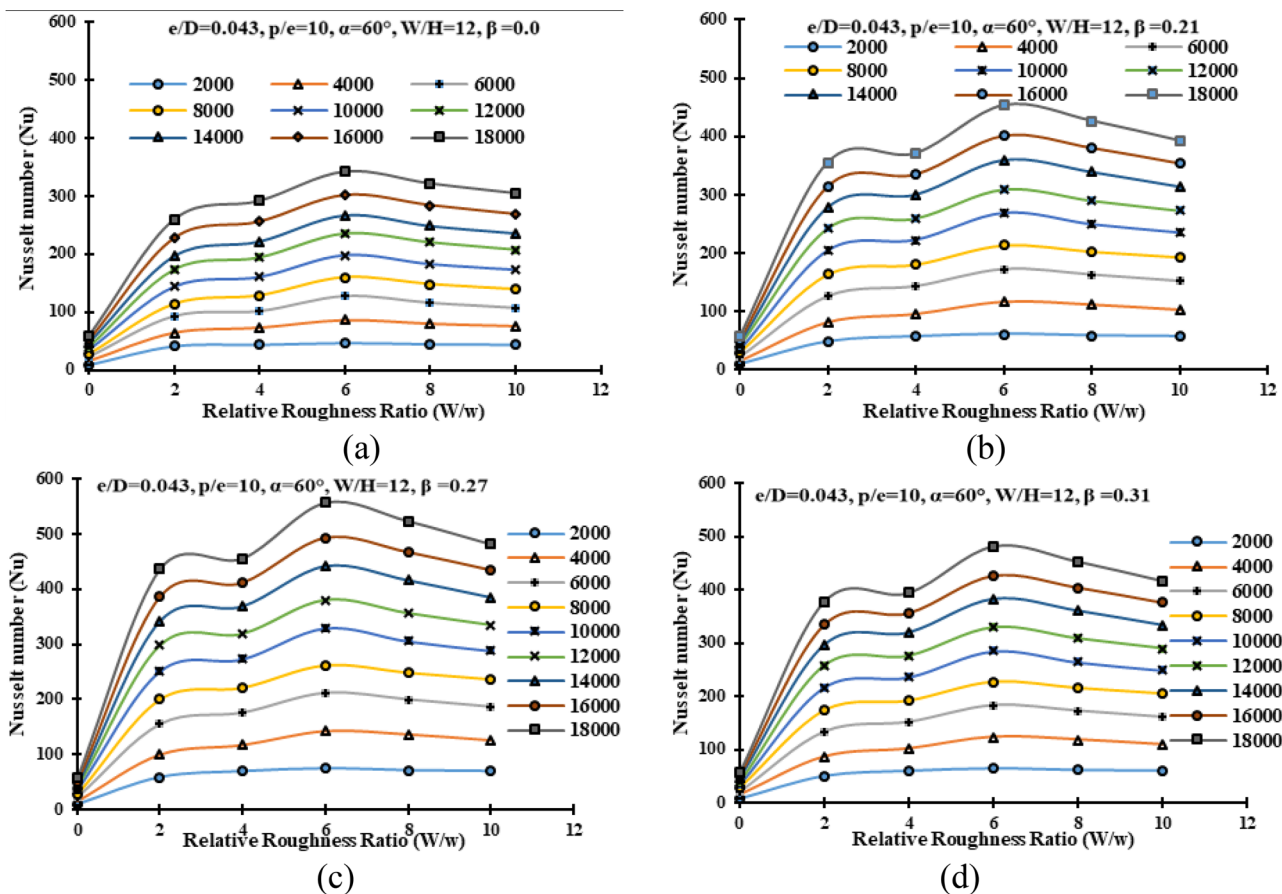


Fig. 9 Nu versus  $W/w$  plots for different  $\beta$  values a 0.0, b 0.21, c 0.27 and d 0.31 in DPPFSAH

5.2.3 Effect of Open Area Ratio ( $\beta$ )

Figure 11A shows Nu increasing as it rises to  $\beta = 0.27$ , then decreasing as it rises again for a further increase in  $\beta$  value. Nu is optimal at  $\beta = 0.27$ , although it is minimal at  $\beta = 0.0$ . The radial development of a secondary flow will be higher at a given linear distance if the perforation diameter is larger. That leads to more fluid flow mixing and reduces the flow zone on the downside of each rib. Once the  $\beta$  value reaches 0.27, the fluid flow through the perforations drops, which may be insufficient to improve the flow through the aperture, resulting in reduced flow turbulence and fluid mixing, and therefore reduced thermal efficacy. The valve can be managed in such a way that the flow passing out of the hole is better mixed, resulting in regional turbulence and improved heat transfer between the flow and the base plate. In the current set of investigations, the optimal THP was obtained by keeping the  $\beta$  value at 0.27. This may be the best value for such a perforated multi-V rib design arrangement and airflow circumstances. Figure 11b depicts the effect of variation in  $\beta$  values on the f value for the same other parameters. Since a greater  $\beta$  value implies fewer resistive forces in fluid flow, the f starts reducing for an increase in  $\beta$  value.

5.2.4 Effect on Nusselt Number and Friction Factor Ratio

Figure 12A, b shows the  $Nu/Nu_s$  and Re relationships in DPPFSAH for different rib combinations and a comparison of SPSAH and DPPFSAH with different  $\beta$  values at  $W/w = 6$ . At  $Re = 6000$ , the perforated rib with  $\beta = 0.27$  attains the maximum value of  $Nu/Nu_s = 9.66$ , which continues for all  $W/w$  values. For further increment in Re values, a sudden decrease in  $Nu/Nu_s$  values which turn into a gradual increase and again achieved optimum values at  $Re = 18,000$ . The plausible explanation behind the underlying phenomenon is that a further increase in  $\beta$  value after  $Re = 6000$  lowers  $Nu/Nu_s$ . This is fair given that roughness-induced air mixing reached its optimal value at  $\beta = 0.27$ , and any further increases in Re levels may interrupt the creation of secondary flow, leading a reduction in  $Nu/Nu_s$ .

Similarly, Fig. 13a, b depicts the influence of Re on  $fff_s$  in DPPFSAH for various  $\beta$  levels and a comparison between SPSAH and DPPFSAH with different  $\beta$  values at  $W/w = 6$ , trends show that  $fff_s$  start decreasing with an increase in  $\beta$  value because of the formation of a decent secondary air-flow via the perforations. The maximum value of  $fff_s$  can be observed as 12.31 at  $\beta = 0.0$ , for  $W/w = 10$  at  $Re = 4000$ .

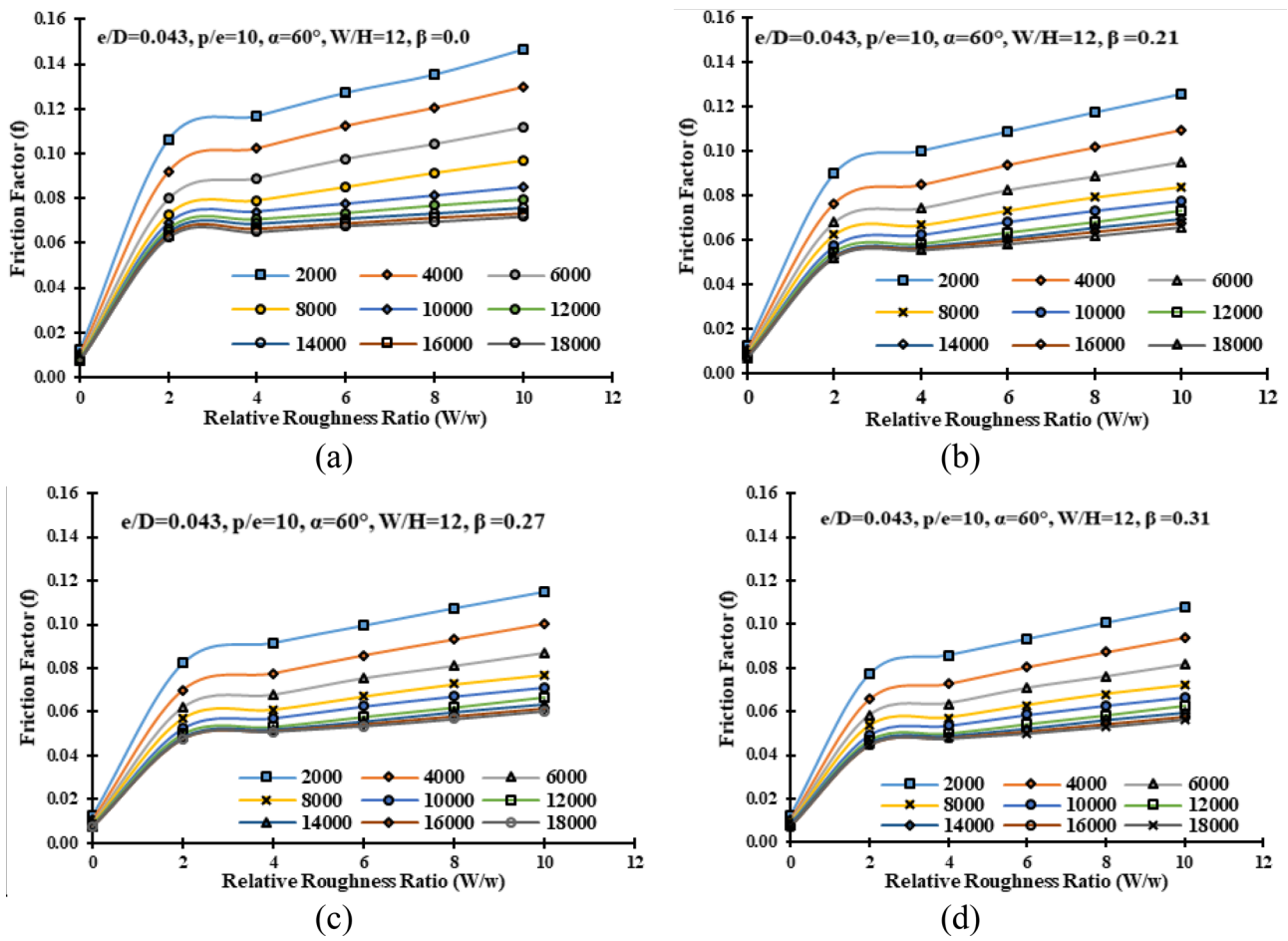


Fig. 10  $f$  versus  $W/w$  plots for different  $\beta$  values a 0.0, b 0.21, c 0.27 and d 0.31 in DPPFSAH

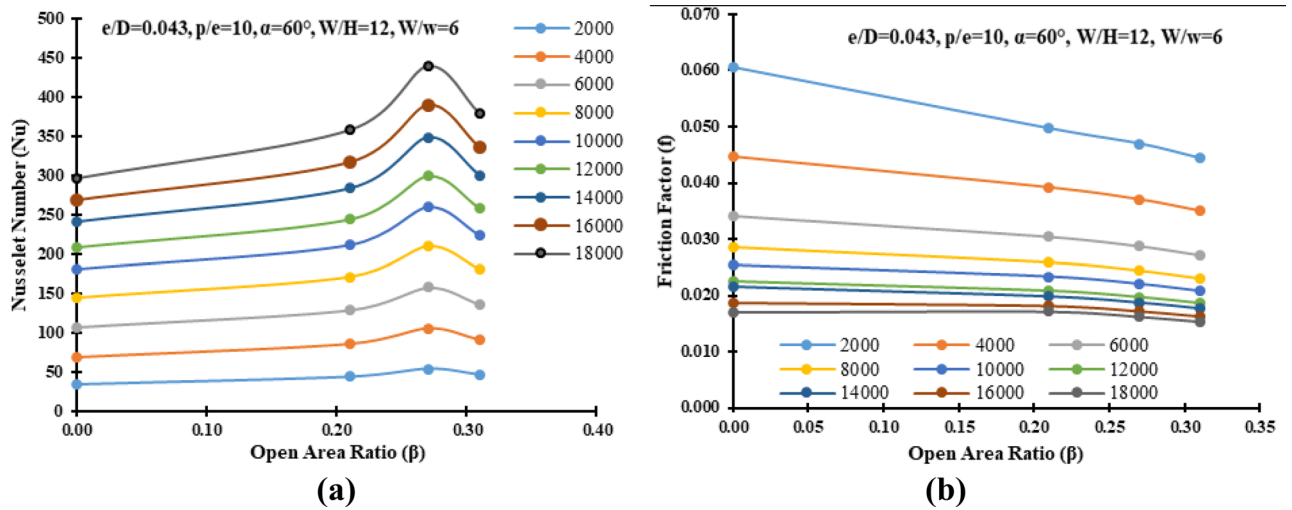


Fig. 11 a  $Nu$  versus  $\beta$  and b  $f$  versus  $\beta$  for different rib combinations in DPPFSAH

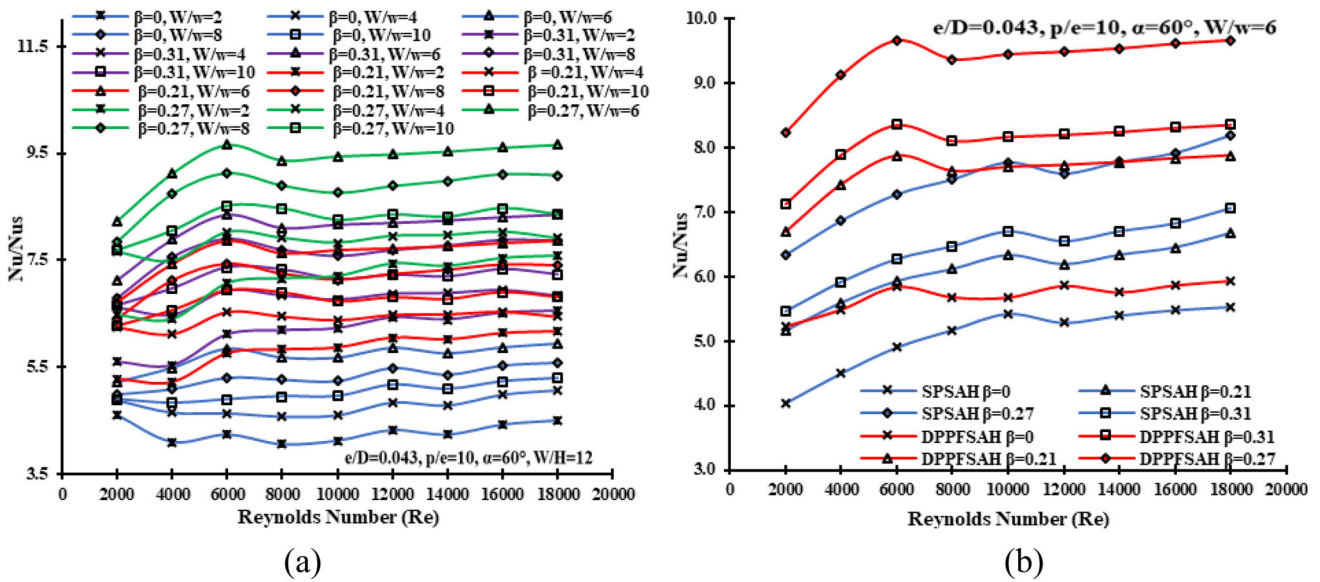


Fig. 12 a  $Nu/Nu_s$  versus  $Re$  for different  $\beta$  in DPPFSAH and b  $Nu/Nu_s$  versus  $Re$  comparison for SPSAH and DPPFSAH with different  $\beta$  values at  $W/w = 6$

### 5.3 Thermohydraulic Performance

The combination of  $Nu$  and  $f$  generates contradictory contexts wherein evaluating the advantages of employing artificial roughness becomes challenging. Hence, Webb and Eckert [43] suggested the thermohydraulic performance parameter (THPP), which equates thermal performance to frictional losses and helps in finding the gain in THPP for suggested roughness as compared to the plain duct for the same power requirements. THPP can be written as:

$$THPP = \left[ \frac{Nu_r}{Nu_s} \right] / \left[ \frac{f_r}{f_s} \right]^{\frac{1}{3}} \tag{16}$$

Further, the concept of the thermal efficiency improvement factor (TEIF) can be invoked to characterize how perforated ribs enhance heat transmission over continuous solid ribs ( $\beta = 0$ ). It may be expressed as:

$$TEIF = \frac{(\eta_{thermal})_{per.} - (\eta_{thermal})_{cont.}}{(\eta_{thermal})_{cont.}} \tag{17}$$

Figure 14a, b depicts the relationship between THPP and TEIF with  $Re$  for various values of  $\beta$  in DPPFSAH, with optimal results obtained in all cases for  $\beta = 0.27$ . The optimum value of THPP for DPPFSAH is 3.96 at  $Re = 14,000$  at  $W/w = 6$ , and the maximum value of TEIF attains a value of 1.33 at  $\beta = 0.27$ ,  $W/w = 2$  and  $Re = 14,000$ , respectively. When compared with the smooth channel, the proposed roughness results in a significant increase in THPP and TEIF numbers.

### 5.4 Correlations for Nu and f for DPPFSAH

To establish the  $Nu$  and  $f$  correlations, the DPPFSAH functional connection has been established for each set of data of  $Nu$  and  $f$ . These are influenced by rib architecture and geometrical variables [44, 45], i.e.  $Re$ ,  $W/w$  and  $\beta$ . For parameters in the ranges of  $\beta = 0.21-0.31$ ,  $W/w = 2-10$  and  $Re = 2000-18,000$ , the correlation is valid.  $Nu$  and  $f$  have the following functional relationships:

$$Nu = f_n(Re, \beta, W/w) \tag{18}$$

$$f = f_n(Re, \beta, W/w) \tag{19}$$

#### 5.4.1 Nusselt Number Correlation

The  $Nu$  correlation was created by applying a regression analysis approach. Figure 15a shows the final correlation for  $Nu$  through curve fitting for experimental data sets and can be expressed as,

$$Nu = 0.0769 \times 10^{-3} (Re)^{0.8953} (\beta)^{0.2417} \left( \frac{W}{w} \right)^{0.1244} \tag{20}$$

#### 5.4.2 Friction Factor Correlation

Figure 15B shows the  $f$  statistics plotted against the operating parameters, and the correlation for the  $f$  could be represented as:

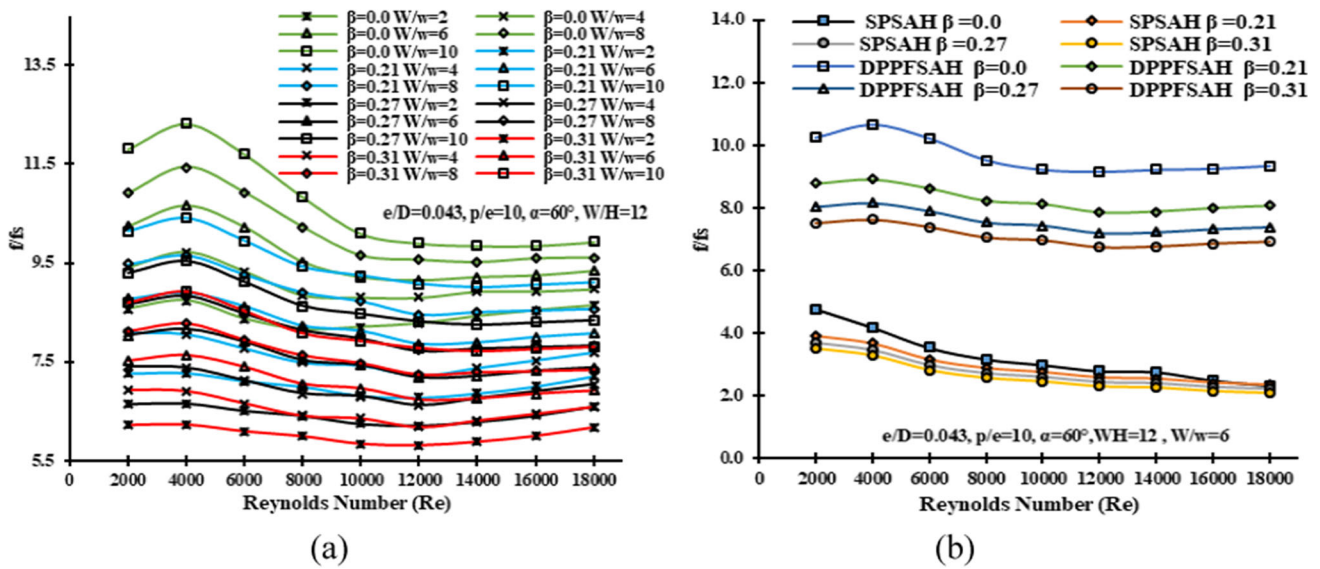


Fig. 13 Influence of Re on  $f/ff_s$  for different  $\beta$  in a DPPFSAH and b comparison of SPSAH and DPPFSAH with different  $\beta$  values at  $W/w = 6$

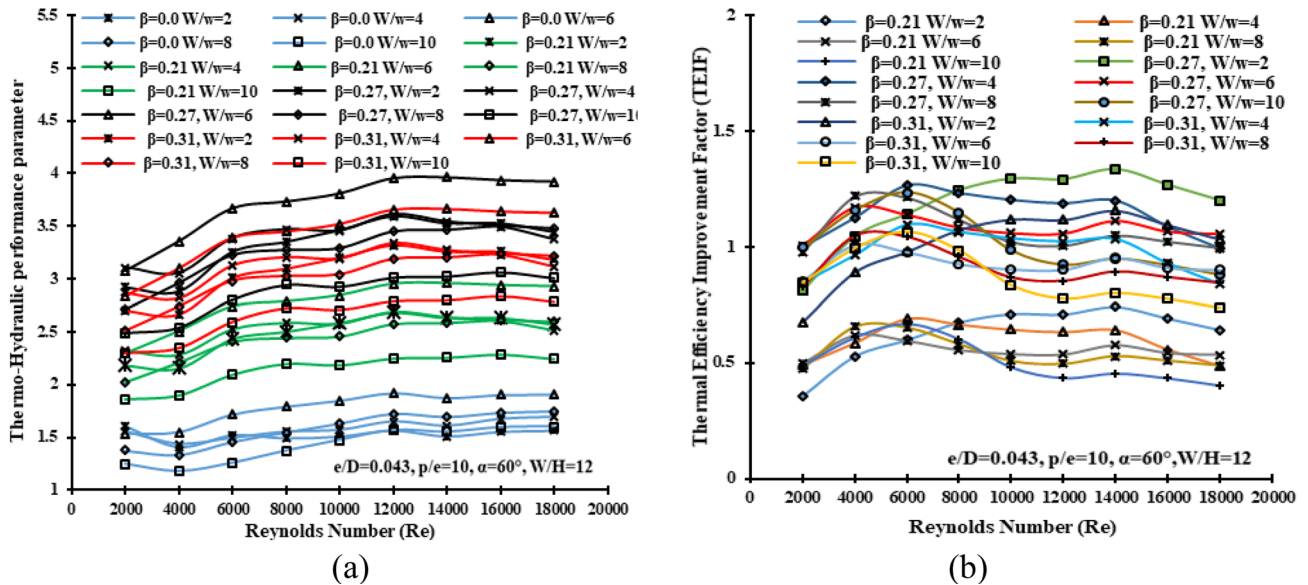


Fig. 14 a THPP versus Re and b TEIF versus Re for different  $\beta$  values in DPPFSAH

$$f = 0.4234 \times 10^{-3} (\text{Re})^{-0.2964} (\beta)^{-0.3897} \left(\frac{W}{w}\right)^{0.1836} \quad (21)$$

Figure 16a, b compares experimental and projected Nu and  $f$  values, revealing that the predicted Nu and  $f$  value are well within  $\pm 14\%$  and  $\pm 7\%$  of the empirical observations. So, the existing correlations may expect Nu and  $f$  for the factors investigated in this work, within acceptable limits.

### 5.5 Comparison of Performance

Table 2 compares optimal values of  $Nu/Nu_s$ ,  $f/ff_s$  and THPP of suggested rib roughness with other comparable rib designs examined by the researcher for DPSAH. Table 2 shows that in the current experimental set-up for a specific range of parameters, ribs having an open area ratio ( $\beta$ ) = 0.27 outperformed the other set-ups compared in this study.

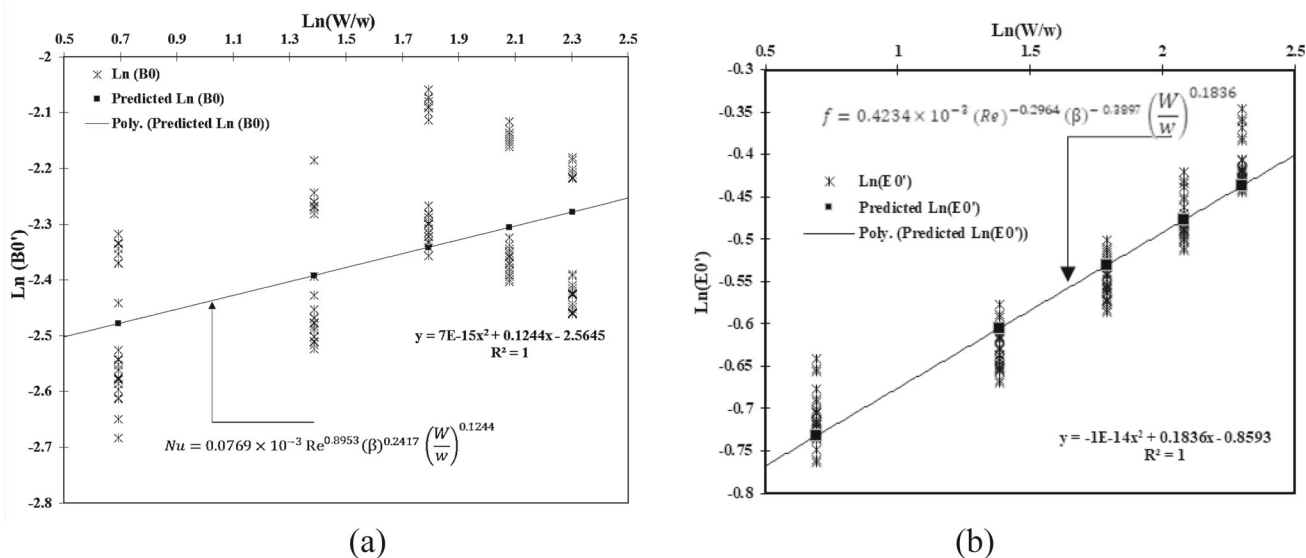


Fig. 15 Correlation equation and trained line for a Nu and b f for DPPFSAH

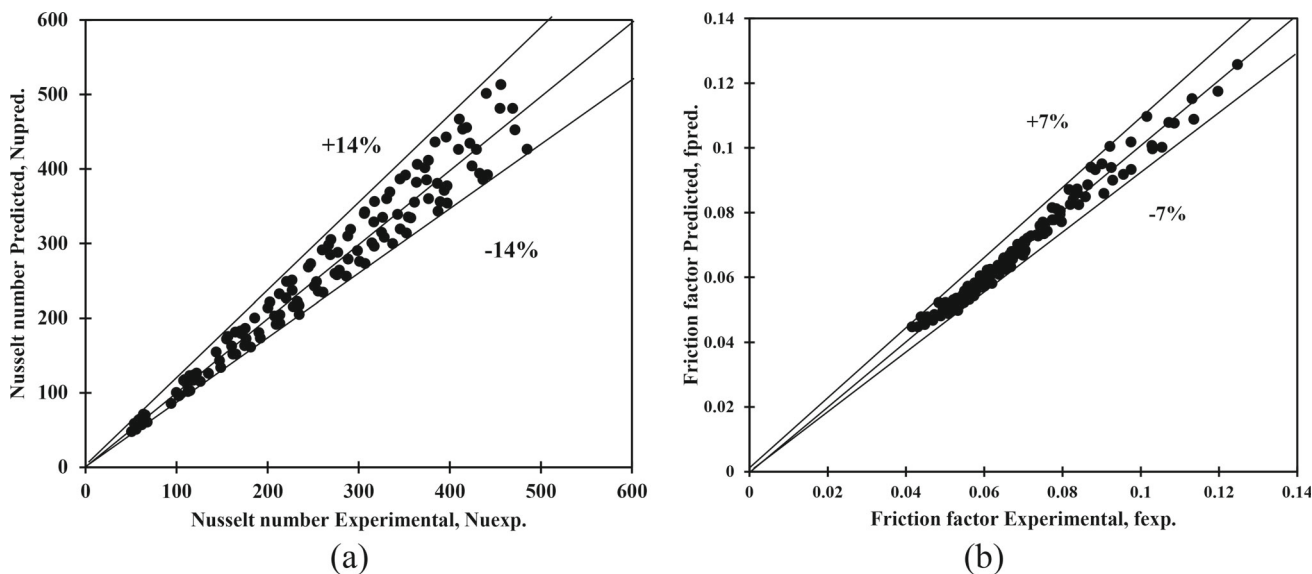


Fig. 16 Comparison of actual and anticipated findings of a Nu, b f for developed a correlation for DPPFSAH

### 6 Conclusions

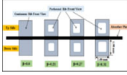
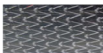


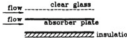
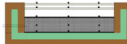
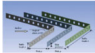
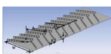
The THPP evaluations and airflow movements in a DPPFSAH duct demonstrate that perforated multi-V ribs created a considerable improvement in performance outcomes over a perforated SPSAH and smooth DPPFSAH, respectively. The following concise summary outlines the findings of the study:

- Increasing the perforation size in multi-V rib DPPFSAH decreases friction losses and reattachment frequency and vortices' dimensions behind the rib, improving fluid mixing and lowering blower power requirements by allowing

secondary flow. It also improves the re-circulation region of flow on the ribs' base, resulting in a higher THPP for the DPPFSAH.

- In DPPFSAH, the optimal performance was reported at an open area ratio ( $\beta$ ) = 0.27 for all four values of  $\beta$  ranging from 0.0 to 0.31.
- The best THPP results were obtained with a relative roughness width ( $W/w$ ) = 6 for five different  $W/w$  values ranging from 2 to 10. For DPPFSAH, the optimum results for  $Nu/Nu_s$ ,  $f/f_s$ , THPP and TEIF were discovered at 9.66, 12.31, 3.96 and 1.33, as compared to the smooth plate, respectively.

**Table 2** Comparative of purposed rib configuration  $Nu/Nu_s, f/f_s$  and THPP with the other comparable published rib shapes for SAH

Researcher	Roughness geometry shape	Pass type	Roughness schematic	Major findings			
				$Nu/Nu_s$	$f/f_s$	THPP	
Current study	Perforated multi-V rib with ( $\beta = 0.0, 0.21, 0.27, 0.31$ )	Parallel flow double pass		$\beta = 0.00$	5.23–5.94	9.21–12.31	1.53–1.90
				$\beta = 0.21$	6.70–7.78	7.85–8.90	2.29–2.93
				$\beta = 0.27$	8.23–9.66	7.19–8.15	3.07–3.96
				$\beta = 0.31$	7.12–8.36	6.73–7.63	2.83–3.66
Ravi and Saini [26]	Multi-V rib desecrate staggered	Counter flow double pass		3.4		2.5	
Tated et al. [46]	Transverse ribs	Counter flow double pass		1.28		1.17	
Sharma et al. [47]	V rib roughness	Counter flow double pass		1.7		1.9	
Metwally et al. [48]	Multi-layer mesh	Parallel flow double pass		–		–	75%
Satyender Singh et al. [49]	Porous media	Wavy channel		–		–	93%
Chamoli and Thakur [50]	Perforated V baffles	Single pass		1.5–3.0		–	–
Jain et al. [51]	Baffles with discrete V perforation	Single pass		4.24		14.73	2.24

**Table 3** Uncertainty interval of various measurements

S. no.	Parameter measured	Symbol	Instrument used	Least count	Uncertainty
1	Duct dimensions:	L	Steel linear scale	1.00 mm	$\pm 1 \text{ mm/1 m}$
	Length	W	Vernier calliper	0.05 mm	$\pm 0.05 \text{ mm}$
	Width	H	Vernier calliper	0.05 mm	$\pm 0.05 \text{ mm}$
	Depth				
2	Flow measurements:		Vernier calliper	0.05 mm	$\pm 0.05 \text{ mm}$
	Pipe diameter Throat diameter		Vernier calliper	0.05 mm	$\pm 0.05 \text{ mm}$
3	Pressure drop measurements:	$(\Delta P)_d$	Micro-manometer	0.001 Pa	$\pm 0.001 \text{ Pa}$
	Across duct Across orifice	$(\Delta P)_o$	U tube manometer	1 mm of kerosene	$\pm 1 \text{ mm}$
4	Atmospheric pressure		Mercury barometer	0.1 mm of Hg	$\pm 0.1 \text{ mm}$
4	Temperature	T	C-type thermocouples	.....	$\pm 0.25 \text{ }^\circ\text{C}$
5	Dimensions of aluminium wire (rib)	e	Vernier calliper	0.05 mm	$\pm 0.05 \text{ mm}$
	Height	w	Vernier calliper	0.05 mm	$\pm 0.05 \text{ mm}$
	Width	p	Vernier calliper	0.05 mm	$\pm 0.05 \text{ mm}$
	Pitch				
6	Current	I	Digital ammeter	0.01 A	$\pm 0.01 \text{ A}$
	Voltage	V	Voltmeter	0.1 V	$\pm 0.1 \text{ V}$
7	Insolation	I	Pyranometer	0.01 mV	$\pm 0.01 \text{ m V}$

- The established correlations will be helpful in determining Nu and  $f$  values that indicate efficient thermal performance and less energy usage, within a set range of  $W/w$ ,  $\beta$  and  $Re$ .

Perforated DPPFSAH outperforms the perforated SPSAH, followed by the continuous DPPFSAH and continuous SPSAH. The observations of the current study show the potential opportunity for the application of perforation in the various proposed rib geometries, so the researcher can examine these roughness for better performance and new optimum values can be drawn for rib roughness parameters of SAH.

### Declarations

**Conflict of interest** “The authors declare that there are no conflicts of interest.”

### Appendix A: Uncertainty Analysis

The list of various measured parameters, instruments used for their measurement with their least counts and uncertainty used is given in Table 3.

Employing empirically collected data including airflow, inlet and exhaust air temperature, solar irradiation and pressure losses, the contributing factors Nu,  $f$  and Re were determined. For error analysis, the current study adopts the Kline and McClintock [39] method. The uncertainty associated with the study of “ $f$ ” is as mentioned below:

$$\frac{\delta f}{f} = \left[ \left( \frac{\delta f}{\partial x_1} \delta x_1 \right)^2 + \left( \frac{\delta f}{\partial x_2} \delta x_2 \right)^2 + \left( \frac{\delta f}{\partial x_3} \delta x_3 \right)^2 + \dots + \left( \frac{\delta f}{\partial x_n} \delta x_n \right)^2 \right]^{0.5}$$

where  $\delta x_1, \delta x_2, \delta x_3, \dots, \delta x_n$  are the potential discrepancies in assessments of  $\times 1, \times 2, \times 3, \dots, x_n$ .

$\delta f$  is known as absolute uncertainty, and  $\delta f/f$  is known as relative uncertainty.

Using Eqs. (8), (11) and (12), uncertainty in Nu, Re and  $f$  can be found as:

Nusselt number (Nu)

$$\frac{\delta N_u}{N_u} = \left[ \left( \frac{\delta h}{h} \right)^2 + \left( \frac{\delta D}{D} \right)^2 + \left( \frac{\delta k}{k} \right)^2 \right]^{0.5} \tag{23}$$

Reynolds number (Re)

$$\frac{\delta R_e}{R_e} = \left[ \left( \frac{\delta V}{V} \right)^2 + \left( \frac{\delta \rho}{\rho} \right)^2 + \left( \frac{\delta D}{D} \right)^2 + \left( \frac{\delta \mu}{\mu} \right)^2 \right]^{0.5} \tag{24}$$

And friction factor ( $f$ )

$$\frac{\delta f}{f} = \left[ \left( -\frac{\delta}{V_d} V_d \right)^2 + \left( -\frac{\delta \rho}{\rho} \right)^2 + \left( \frac{\delta D}{D} \right)^2 + \left( -\frac{\delta}{L} L \right)^2 + \left( \frac{\delta(\Delta P_d)}{\Delta P_d} \right)^2 \right]^{0.5} \tag{25}$$

### References

1. Lu, J.; He, G.; Mao, F.: Solar seasonal thermal energy storage for space heating in residential buildings: optimization and comparison with an air-source heat pump. *Energy Sources Part B Econ. Plan. Policy* **00**(00), 279–296 (2020). <https://doi.org/10.1080/15567249.2020.1786192>
2. Saini, M.; Sharma, A.; Singh, V.P.; Dwivedi, G.; Jain, S.: Solar thermal receivers—a review. *Adv. Mater. Manuf. Energy Eng.* **2**, 310–325 (2022). <https://doi.org/10.1007/978-981-16-8341-1>
3. Ghritlahre, H.K.; Verma, M.: Solar air heaters performance prediction using multi-layer perceptron neural network—a systematic review. *Energy Sources Part A Recover. Util. Environ. Eff.* **00**(00), 1–18 (2021). <https://doi.org/10.1080/15567036.2021.1923869>
4. Arunkumar, H.S., et al.: Review on the design modifications of a solar air heater for improvement in the thermal performance. *Sustain. Energy Technol. Assessments* **39**(January), 1–29 (2020). <https://doi.org/10.1016/j.seta.2020.100685>
5. Dutt, N.; Binjola, A.; Hedau, A.J.; Kumar, A.; Singh, V.P.; Meena, C.S.: Comparison of CFD results of smooth air duct with experimental and available equations in literature. *Int. J. Energy Resour. Appl.* **1**(1), 40–47 (2022). <https://doi.org/10.56896/IJERA.2022.1.1.006>
6. Alam, T.; Kim, M.-H.: Heat transfer enhancement in solar air heater duct with conical protrusion roughness ribs. *Appl. Therm. Eng.* **126**, 458–469 (2017). <https://doi.org/10.1016/j.applthermaleng.2017.07.181>
7. Singh, S.: Experimental and numerical investigations of a single and double pass porous serpentine wavy wiremesh packed bed solar air heater. *Renew. Energy* **145**, 1361–1387 (2020). <https://doi.org/10.1016/j.renene.2019.06.137>
8. Al-Damook, M.; Obaid, Z.A.H.Z.A.H.; Al Qubeissi, M.; Dixon-Hardy, D.; Cottom, J.; Heggs, P.J.P.J.: CFD modeling and performance evaluation of multipass solar air heaters. *Numer. Heat Transf. Part A Appl.* **76**(6), 438–464 (2019). <https://doi.org/10.1080/10407782.2019.1637228>
9. Ho, C.D.; Hsiao, C.F.; Chang, H.; Tien, Y.E.: Investigation of device performance for recycling double-pass V-corrugated solar air collectors. *Energy Procedia* **105**, 28–34 (2017). <https://doi.org/10.1016/j.egypro.2017.03.275>
10. Fudholi, A.; Sopian, K.; Ruslan, M.H.; Othman, M.Y.; Yahya, M.: Thermal efficiency of double pass solar collector with longitudinal fins absorbers. *Am. J. Appl. Sci.* **8**(3), 254–260 (2011). <https://doi.org/10.3844/ajassp.2011.254.260>
11. Singh, V.P., et al.: Heat transfer and friction factor correlations development for double pass solar air heater artificially roughened with perforated multi-V ribs. *Case Stud. Therm. Eng.* **39**, 102461 (2022). <https://doi.org/10.1016/j.csite.2022.102461>
12. Singh, V.P., et al.: Recent developments and advancements in solar air heaters : a detailed review. *Sustainability* **14**(19), 1–57 (2022). <https://doi.org/10.3390/su141912149>



13. Goel, V., et al.: A comprehensive study on the progressive development and applications of solar air heaters. *Sol. Energy* **229**(July), 112–147 (2021). <https://doi.org/10.1016/j.solener.2021.07.040>
14. Kumar, A.; Sharma, S.; Kumar, S.; Maithani, R.: Thermohydraulic analysis of twisted tape inserts with SiO<sub>2</sub>/H<sub>2</sub>O nanofluid in heat exchanger. *Aust. J. Mech. Eng.* **00**(00), 1–14 (2021). <https://doi.org/10.1080/14484846.2021.1960672>
15. Maithani, R.; Sharma, S.; Kumar, A.: Thermo-hydraulic and exergy analysis of inclined impinging jets on absorber plate of solar air heater. *Renew. Energy* **179**, 84–95 (2021). <https://doi.org/10.1016/j.renene.2021.07.013>
16. Maithani, R.; Kumar, B.; Sharma, S.; Kumar, S.; Kumar, A.: Effect of a unique winglet twisted tape insert on thermal and hydraulic properties of tubular heat exchanger. *Exp. Heat Transf.* **00**(00), 1–22 (2022). <https://doi.org/10.1080/08916152.2022.2038725>
17. Kumar, B.; Patil, A.K.; Jain, S.; Kumar, M.: Effects of double V cuts in perforated twisted tape insert: an experimental study. *Heat Transf. Eng.* **41**(17), 1473–1484 (2020). <https://doi.org/10.1080/01457632.2019.1649926>
18. Kumar, R.; Kumar, A.; Goel, V.: Performance improvement and development of correlation for friction factor and heat transfer using computational fluid dynamics for ribbed triangular duct solar air heater. *Renew. Energy* **131**, 788–799 (2019). <https://doi.org/10.1016/j.renene.2018.07.078>
19. Sharma, S.; Das, R.K.; Kulkarni, K.: Computational and experimental assessment of solar air heater roughened with six different baffles. *Case Stud. Therm. Eng.* **27**(1–18), 101350 (2021). <https://doi.org/10.1016/j.csite.2021.101350>
20. Kumar, R.; Goel, V.; Bhattacharyya, S.; Tyagi, V.V.; Abusorrah, A.M.: Experimental investigation for heat and flow characteristics of solar air heater having symmetrical gaps in multiple-arc rib pattern as roughness elements. *Exp. Heat Transf.* (2021). <https://doi.org/10.1080/08916152.2021.1905752>
21. Arya, N., Kumar, R., Goel, V.: Role of artificial roughness in the performance improvement of solar air heaters. In: *Green Energy and Technology*, pp. 555–578 (2022) [https://doi.org/10.1007/978-981-16-2648-7\\_23](https://doi.org/10.1007/978-981-16-2648-7_23)
22. Sharma, A.; Bharadwaj, G.; Varun: Heat transfer and friction factor correlation development for double-pass solar air heater having V-shaped ribs as roughness elements. *Exp. Heat Transf.* **30**(1), 77–90 (2017). <https://doi.org/10.1080/08916152.2016.1161676>
23. Alam, T.; Saini, R.P.; Saini, J.S.: Effect of circularity of perforation holes in V-shaped blockages on heat transfer and friction characteristics of rectangular solar air heater duct. *Energy Convers. Manag.* **86**(00), 952–963 (2014). <https://doi.org/10.1016/j.enconman.2014.06.050>
24. Alam, T.; Meena, C.S.; Balam, N.B.; Kumar, A.; Cozzolino, R.: Thermo-hydraulic performance characteristics and optimization of protrusion rib roughness in solar air heater. *Energies* **14**(11), 1–21 (2021). <https://doi.org/10.3390/en14113159>
25. Ravi, R.K.; Saini, R.P.: Effect of roughness elements on thermal and thermohydraulic performance of double pass solar air heater duct having discrete multi V-shaped and staggered rib roughness on both sides of the absorber plate. *Exp. Heat Transf.* **6152**(1), 47–67 (2017). <https://doi.org/10.1080/08916152.2017.1350217>
26. Ravi, R.K.; Saini, R.P.: Experimental investigation on performance of a double pass artificial roughened solar air heater duct having roughness elements of the combination of discrete multi V shaped and staggered ribs. *Energy* **116**, 507–516 (2016). <https://doi.org/10.1016/j.energy.2016.09.138>
27. Kaur, I.; Singh, P.: Heat and flow characteristics of V-shaped protrusion/concavity combined with miniature V-ribs. *Numer. Heat Transf. Part A Appl.* (2020). <https://doi.org/10.1080/10407782.2020.1793549>
28. Kumar, B.; Kumar, M.; Patil, A.K.; Jain, S.: Effect of V cut in perforated twisted tape insert on heat transfer and fluid flow behavior of tube flow: an experimental study. *Exp. Heat Transf.* **32**(6), 524–544 (2019). <https://doi.org/10.1080/08916152.2018.1545808>
29. Thakur, S., Thakur, N.S.: Impact of multi-staggered rib parameters of the ‘W’ shaped roughness on the performance of a solar air heater channel. In: *Energy Sources, Part A: Recovery, Utilization, and Environmental Effects*, pp. 1–20 (2020). <https://doi.org/10.1080/15567036.2020.1764672>
30. Singh, V.P.; Jain, S.; Gupta, J.M.L.: Analysis of the effect of perforation in multi-v rib artificial roughened single pass solar air heater: part A. *Exp. Heat Transf.* (2021). <https://doi.org/10.1080/08916152.2021.1988761>
31. Singh, V.P.; Jain, S.; Gupta, J.M.L.: Performance assessment of double-pass parallel flow solar air heater with perforated multi-V ribs roughness—part B. *Exp. Heat Transf.* **00**(00), 1–18 (2022). <https://doi.org/10.1080/08916152.2021.2019147>
32. Singh, V.P.; Jain, S.; Gupta, J.M.L.: Analysis of the effect of variation in open area ratio in perforated multi-V rib roughened single pass solar air heater—part A. *Energy Sour. Part A Recover Util. Environ. Effects* **44**, 1–21 (2022). <https://doi.org/10.1080/15567036.2022.2029976>
33. Singh, V.P.; Jain, S.; Karn, A.; Kumar, A.; Dwivedi, G.: Mathematical modeling of efficiency evaluation of double pass parallel flow solar air heater. *Sustainability* **14**(17), 1–22 (2022). <https://doi.org/10.3390/su141710535>
34. Hernández, A.L.; Quiñonez, J.E.: Analytical models of thermal performance of solar air heaters of double-parallel flow and double-pass counter flow. *Renew. Energy* **55**, 380–391 (2013). <https://doi.org/10.1016/j.renene.2012.12.050>
35. Ashok Kumar, B., et al.: Thermohydraulic performance of solar air heater with staggered multiple V-shaped ribs on the absorber plate. *Energy* **8**(1), 387–400 (2017). <https://doi.org/10.1016/j.rser.2016.11.192>
36. Ong, K.S.S.: Thermal performance of solar air heaters: mathematical model and solution procedure. *Sol. Energy* **55**(2), 93–109 (1995). [https://doi.org/10.1016/0038-092X\(95\)00021-1](https://doi.org/10.1016/0038-092X(95)00021-1)
37. Gupta, D.; Solanki, S.C.; Saini, J.S.: Heat and fluid flow in rectangular solar air heater ducts having transverse rib roughness on absorber plates. *Sol. Energy* **51**(1), 31–37 (1993). [https://doi.org/10.1016/0038-092X\(93\)90039-Q](https://doi.org/10.1016/0038-092X(93)90039-Q)
38. Hans, V.S.; Saini, R.P.; Saini, J.S.: Heat transfer and friction factor correlations for a solar air heater duct roughened artificially with multiple v-ribs. *Sol. Energy* **84**(6), 898–911 (2010). <https://doi.org/10.1016/j.solener.2010.02.004>
39. Kline, S.J.: The purposes of uncertainty analysis. *J. Fluids Eng.* **107**, 153–160 (1985)
40. Kwak, J.S.; Shin, S.: Effect of hole shape on the heat transfer in a rectangular duct with perforated blockage walls. *J. Mech. Sci. Technol.* **22**(April), 1945–1951 (2008). <https://doi.org/10.1007/s12206-008-0736-7>
41. Vogiatzis, I.I.; Denizopoulou, A.C.; Ntinis, G.K.; Fragos, V.P.: Simulation analysis of air flow and turbulence statistics in a rib grit roughened duct. *Sci. World J.* (2014). <https://doi.org/10.1155/2014/791513>
42. Tariq, A.; Panigrahi, P.K.; Muralidhar, K.: Flow and heat transfer in the wake of a surface-mounted rib with a slit. *Exp. Fluids* **37**(5), 701–719 (2004). <https://doi.org/10.1007/s00348-004-0861-8>
43. Webb, R.L.; Eckert, E.R.G.: Application of rough surfaces to heat exchanger. *Int. J. Heat Mass Transf.* **15**, 1647–1658 (1972)
44. Saini, S.K.; Saini, R.P.: Development of correlations for Nusselt number and friction factor for solar air heater with roughened duct having arc-shaped wire as artificial roughness. *Sol. Energy* **82**(12), 1118–1130 (2008). <https://doi.org/10.1016/j.solener.2008.05.010>
45. Singh, V.P.; Jain, S.; Kumar, A.: Establishment of correlations for the Thermo-Hydraulic parameters due to perforation in a multi-V

- rib roughened single pass solar air heater. *Exp. Heat Transf.* **35**(5), 1–20 (2022). <https://doi.org/10.1080/08916152.2022.2064940>
46. Tated, M.K.; Singh, D.P.; Dogra, S.: Heat transfer and friction factor characteristics of double pass solar air heater using W-shaped artificial roughness ribs. *J. Mech. Civ. Eng.* **5**(3), 25–30 (2015)
  47. Sharma, A.; Goel, V.; Bharadwaj, G.: Heat transfer and friction characteristics of double pass solar air heater having V-shaped roughness on the absorber plate. *J. Renew. Sustain. Energy* **5**(2014), 1–15 (2013). <https://doi.org/10.1063/1.4794747>
  48. Metwally, M.N.; Abouziyan, H.Z.; Elleathy, A.M.: Performance of advanced corrugated-duct solar air collector compared with five conventional designs. *Renew. Energy* **10**(4), 519–537 (1997)
  49. Singh, S.; Chaurasiya, S.K.; Negi, B.S.: “Efficient design of a wavy channel embedded with porous media for solar air heating. *Energy Sour. Part A Recover. Util. Environ. Effects* **00**(00), 1–17 (2020). <https://doi.org/10.1080/15567036.2020.1850930>
  50. Chamoli, S.; Thakur, N.S.S.: Correlations for solar air heater duct with V-shaped perforated baffles as roughness elements on absorber plate. *Int. J. Sustain. Energy* **35**, 37–41 (2013). <https://doi.org/10.1080/14786451.2013.857318>
  51. Jain, S.K.; Misra, R.; Kumar, A.; Agrawal, G.D.: Thermal performance investigation of a solar air heater having discrete V-shaped perforated baffles. *Int. J. Ambient Energy* **43**, 1–10 (2019). <https://doi.org/10.1080/01430750.2019.1636874>

Springer Nature or its licensor (e.g. a society or other partner) holds exclusive rights to this article under a publishing agreement with the author(s) or other rightsholder(s); author self-archiving of the accepted manuscript version of this article is solely governed by the terms of such publishing agreement and applicable law.